Vertical coupling and transition energies in multilayer InAs/GaAs quantum-dot structures

S. Taddei
Istituto Nazionale per la Fisica della Materia, and Dipartimento di Fisica, largo Enrico Fermi 2, I-50125, Firenze, Italy

M. Colocci and A. Vinattieri
Istituto Nazionale per la Fisica della Materia, Dipartimento di Fisica, and LENS, largo Enrico Fermi 2, I-50125, Firenze, Italy

F. Bogani
Istituto Nazionale per la Fisica della Materia, and Dipartimento di Energetica, via S. Marta 3, I-50139, Firenze, Italy

S. Franchi, P. Frigeri, L. Lazzarini, and G. Salviati
CNR-MASPEC, Parco delle Scienze 37a, I-43010, Fontanini, Parma, Italy
(Received 14 October 1999; revised manuscript received 23 February 2000)

Vertically ordered quantum dots in multilayer InAs/GaAs structures have attracted large interest in recent years for device application as light emitters. Contradictory claims on the dependence of the fundamental transition energy on the interlayer separation and number of dot layers have been reported in the literature. We show that either a blueshift or a redshift of the fundamental transition energy can be observed in different coupling conditions and straightforwardly explained by including strain, indium segregation, and electron-hole Coulomb interaction, in good agreement with experimental results.

INTRODUCTION

The interest in the fabrication of diode lasers emitting in the 1.3-μm wavelength range has steadily increased in the last few years due to the fact that such lasers are key components of fiber-optic-based communication networks. In particular, quantum-dot (QD) structures obtained through the self-organized growth of three-dimensional islands of InAs on a GaAs substrate are currently considered highly promising candidates for photonic applications at 1.3 μm. In fact, reduction of the ground-state transition energy of the QD's toward the 1.3-μm region has been already demonstrated when the dots are deposited by atomic layer molecular beam epitaxy (ALMBE) rather than standard molecular beam epitaxy[1] (MBE); further tuning of the fundamental transition energy has been shown to be possible in multilayer structures, obtained by successive deposition of InAs QD layers separated by GaAs spacers of appropriate thickness, due to the possibility of controlling the electronic coupling among electrons and holes in the strain-induced vertical ordering of the dots into wirelike dot columns.[2,3] We want to show that the interplay of strain and electron-hole Coulomb interaction can result in an increase or in a decrease of the ground-state transition energy for an increasing number of dot layers, depending on the thickness of the GaAs spacer layers. We also show that the experimental results for the ground-state transition energies, as obtained from the photoluminescence spectra, can be nicely reproduced within a simple theoretical model for the calculation of the electronic states in these systems once strain, indium segregation,[4] and Coulomb effects are duly taken into account.

I. SAMPLES AND EXPERIMENTAL DATA

The InAs/GaAs QD structures were grown by ALMBE. They consist of stacked layers of InAs QD's separated by GaAs spacer layers. The samples differ for the number N embedded of QD layers ($N=1-9$) and the thickness D of the GaAs spacers ($D=5.6-15$ nm). The GaAs buffers were deposited at 600 °C by MBE in order to optimize the morphology; the growth was interrupted for 210 s before and after the deposition of each InAs cycle to stabilize the ALMBE growth temperature of the InAs QD's (460 °C) and of the GaAs spacers (360 °C). The low growth temperature of the spacers was chosen in order to reduce the interaction between QD's and upper confining layers. The InAs coverage was 3 monolayers (ML) in all the layers. A transmission electron microscopy (TEM) (110) cross-section of a QD structure with five embedded layers of InAs QD's separated by 10-nm-thick GaAs spacers is shown in Fig. 1. Moreover, we point out that in a statistical analysis of the TEM images we observe both stacked QD's with the same size and stacked QD's with sizes that slightly increase as we move to the upper layers (actually, the QD height is more or less constant, while the diameter increases), but the latter case seems more frequent.

The photoluminescence (PL) spectra were taken, after excitation of the sample, with a frequency-doubled Nd:yttrium-aluminum-garnet laser, by using standard photon-counting techniques. A Hamamatsu photomultiplier tube (PMT) with $In_xGa_{1-x}As$ photocathode was used for photon detection. The samples were mounted in a cold-finger cryostat operating between 10 and 300 K. We plot in Fig. 2 the fundamental transition energies versus the number of QD layers at 10 K, for different layer separations ($D=5.6$ nm, squares; $D=10$ nm, circles; $D=15$ nm, diamonds).

Either a blueshift or a redshift of the PL peak depending on the spacer thickness, for increasing number of the stacked QD layers, is clearly observed. We refer the reader to Ref. 5 for details on the PL spectra.

 ©2000 The American Physical Society

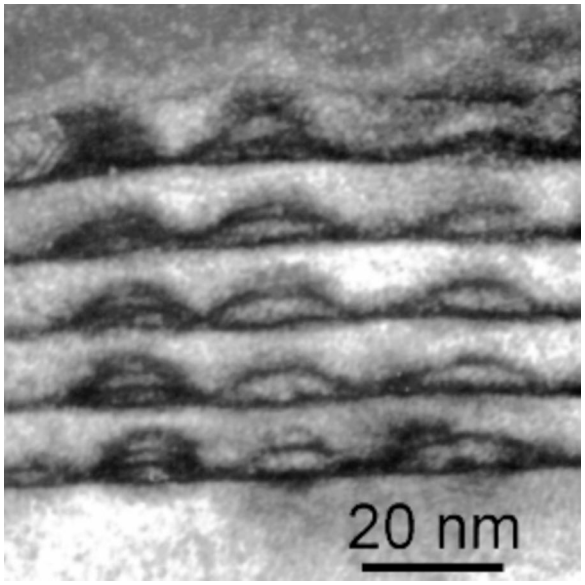

FIG. 1. (110) cross-sectional TEM image of a structure consisting of $N=5$ embedded layers of InAs QD's, separated by 10-nm-thick GaAs spacers. The image was taken under (002) dark field conditions that enhance the compositional contrast between InAs and GaAs.

II. MODEL AND NUMERICAL METHOD

The simplest model for describing a single $In_xGa_{1-x}As/GaAs$ QD is an envelope function approximation using a one-band Hamiltonian with constant effective masses, and a three-dimensional potential that has the same geometrical shape of the QD and includes a constant[6] or numerically computed[7] strain contribution. More recent models are based on multiband $\mathbf{k}\cdot\mathbf{p}$ Hamiltonians and realistic strain distributions.[8–11] Furthermore, an alternative approach is based on pseudopotential calculations.[12–14] Finally, indium segregation effects and the Coulomb interaction must be considered.

Here, we adopt the following approach. We use a one-band Hamiltonian with constant effective masses. Moreover, an analytical approximation of a realistic strain distribution is used, and also the indium segregation is taken into account. Finally, the Coulomb interaction is computed perturbatively. The one-band approximation gives significative differences in the calculation of the excited states, but only small corrections for the ground states;[8,9] since here we are interested only to the latter, this simplified approach is justified.

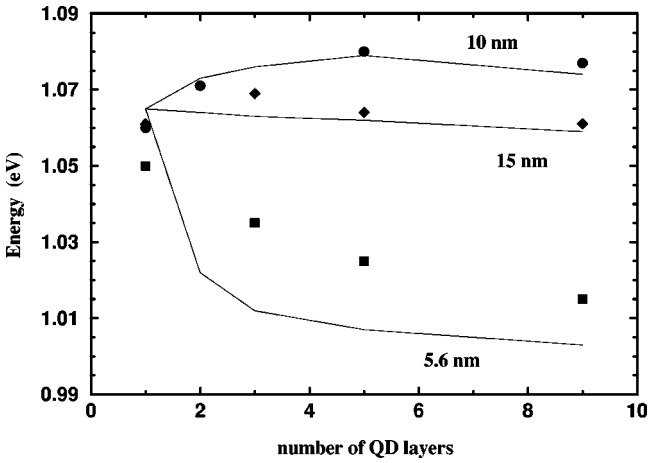

FIG. 2. Experimental transition energies (points), at $T=10$ K, and calculated transition energies (lines) with Coulomb corrections versus the number of QD layers for different layer separations.

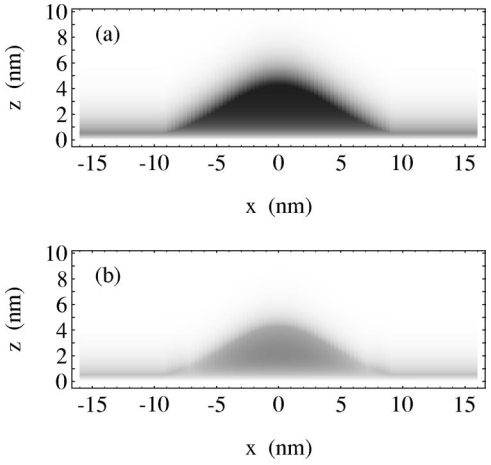

FIG. 3. Confinement potential for a single QD (indium segregation length $\simeq$3 ML) for (a) electrons and (b) heavy holes in the (100) plane through the top of the dot. The gray scale is the same for all plots.

A. Potential model

The potential is defined as follows. We suppose that the QD has a cylindrical symmetry and a Gaussian height profile with standard deviation σ and maximum height h (in fact, the shape and the dimension of the QD's depend on the growth conditions and, for example, QD's with either cylindrical[17–19] or pyramidal[7,10,16] symmetries can be obtained). Moreover, we must take into account that the QD resides on a continuous wetting layer with thickness d. The confinement potential for a single QD can be written as

$$V^e(\rho,z)=E_c(x(z,S(\rho)),z,S(\rho))-E_c(0,z,S(\rho)), \quad (1)$$

$$V^{hh}(\rho,z)=E_v^{hh}(0,z,S(\rho))-E_v^{hh}(x(z,S(\rho)),z,S(\rho)), \quad (2)$$

$$V^{lh}(\rho,z)=E_v^{lh}(0,z,S(\rho))-E_v^{lh}(x(z,S(\rho)),z,S(\rho)), \quad (3)$$

where $x(z,S(\rho))$ is the indium composition, depending both on the nominal composition, and the indium segregation length,[4] while the functions E_c, E_v^{hh}, and E_v^{lh}, are the edges of the energy bands of the $In_xGa_{1-x}As$. For a more detailed discussion, and a definition of the previous functions, see Ref. 15. In Fig. 3, we show the density plots of the single QD potential.

The potential for the QD array is the sum of a given number of single QD potentials shifted by the layer separation. The model is a good approximation when the separation is not too small and the QD islands are well defined and distinct; otherwise the strain effects modify the single QD potential. In this case, however, the simple superposition of the single QD potentials still should be a reasonable approximation, and should give qualitatively correct results. As

shown in Ref. 20, no major deviations are expected from the results obtained by superposing the strain fields acting on isolated dots, as assumed in our calculations, where the interaction of the QD strain fields has been neglected, as long as the dot separation exceeds 2–3 nm as in our case. Moreover, as shown in Ref. 20 no further contribution is given by the piezoelectric field to the ground-state electronic energies.

Furthermore, according to the TEM images, we assumed that the QD heights are constant, while the aspect ratio (QD height to base size ratio) slightly decreases as we move to the upper layer. Finally, the potential parameters (island dimension, aspect ratio variation, and segregation length) have been fixed in order to fit both the structural properties (TEM) and the photoluminescence spectra. Once the potential is defined, the transition energies are computed as $\Delta E_\alpha = E_\alpha^e + E_\alpha^{hh\,(lh)} + E_g^{\mathrm{GaAs}} + E_C$, where E_α^e and $E_\alpha^{hh\,(lh)}$ are the single-particle confinement energies, E_g^{GaAs} is the energy gap between the valence and conduction bands of the GaAs, and E_C is the Coulomb energy.

B. Bound state computation

The computation of the bound states of a general multiwell three-dimensional potential, where slight tunneling effects must be taken into account, is not a simple task. Here we use the Green function deterministic numerical method,[15,21,22] (GFDNM) which has the following useful properties: (a) it has very good accuracy for tunneling problems; (b) the propagator for a multidimensional quantum system can be factorized as a tensorial product of one-dimensional matrices multiplied by a diagonal tensor, with much less effort both in terms of CPU time and memory requirements; (c) we can choose an appropriate distribution of grid points, according to the shapes of the wave functions, in order to obtain good accuracy with a quite small number of points. In the following, we give a brief description of the method. A more detailed discussion can be found in the references given above.

The short time propagator, $K(\mathbf{r},\mathbf{r}';\varepsilon)$, determines the evolution of a quantum system in a small time interval ε, relating the wave function ψ at the time $t_0+\varepsilon$ to the wave function at the time t_0, by

$$\psi(\mathbf{r};t_0+\varepsilon) = \int \cdots \int K(\mathbf{r},\mathbf{r}';\varepsilon)\, \psi(\mathbf{r}';t_0)\, d\mathbf{r}'. \tag{4}$$

For the computation of the bound states, it is convenient to use the Euclidean formulation (imaginary time), because the numerical integrations are more stable and accurate. In the following, therefore, $K(\mathbf{r},\mathbf{r}';\varepsilon)$ denotes the Euclidean short time propagator. If we now consider the case of a three-dimensional potential with a cylindrical symmetry, the propagator can be written in the following way:

$$K(\mathbf{r},\mathbf{r}';\varepsilon) = \sum_{m=-\infty}^{+\infty} \frac{1}{\sqrt{\rho\rho'}} g_m(\rho,z,\rho',z';\varepsilon) \frac{1}{2\pi} e^{im(\theta-\theta')}, \tag{5}$$

where $\mathbf{r} \equiv (\rho,\theta,z)$ are the cylindrical coordinates. Since the azimuthal quantum number m is conserved, the contributions of different values of m can be separated. In fact, if we define the cylindrical wave functions $\phi_{(\alpha m)}(\rho,z)$, by

$$\psi_{(\alpha m)}(\mathbf{r}) = \frac{\phi_{(\alpha m)}(\rho,z)}{\sqrt{\rho}} \frac{e^{im\theta}}{2\pi}, \tag{6}$$

where $\psi_{(\alpha m)}(\mathbf{r})$ are the complete eigenfunctions of the Hamiltonian, they satisfy the integral equation

$$\int \int g_m(\rho,z,\rho',z';\varepsilon)\phi_{(\alpha m)}(\rho',z')d\rho' dz' = e^{-\varepsilon E_{(\alpha m)}}\phi_{(\alpha m)}(\rho,z). \tag{7}$$

Equation (7) can be approximated by

$$\sum_{j_1=1}^{M_\rho} \sum_{j_2=1}^{M_z} (\tilde{g}_m^\varepsilon)_{i_1,i_2,j_1,j_2} \phi_{(\alpha m)}^{j_1,j_2} \simeq e^{-\varepsilon E_{(\alpha m)}} \phi_{(\alpha m)}^{i_1,i_2}, \tag{8}$$

where

$$(\tilde{g}_m^\varepsilon)_{i_1,i_2,j_1,j_2} \equiv \int \int g_m(\rho_{i_1},z_{i_2},\rho',z';\varepsilon) \times l_{j_1}(\rho'),l_{j_2}(z')d\rho' dz' \tag{9}$$

and the functions $l_i(x)$ are interpolating functions [we use piecewise polynomials; in such a case, the coefficients $\phi_{(\alpha m)}^{i_1,i_2}$ are just the values of the cylindrical wave function in the grid points (ρ_{i_1},z_{i_2})]. If the functions $l_i(x)$ and the propagator are given, the integrals (9) can be calculated by analytical or numerical techniques. Unfortunately, an explicit general expression for the finite time propagator does not exist. However, an approximate expression for the short time cylindrical propagator, correct up to $O(\varepsilon)$, is given by

$$g_m(\rho,z,\rho',z';\varepsilon) = k_m^\rho(\rho,\rho';\varepsilon)k^z(z,z';\varepsilon)e^{-\varepsilon V(\rho,z)}, \tag{10}$$

where

$$k_m^\rho(\rho,\rho';\varepsilon) = \sqrt{\frac{m_\rho}{2\pi\varepsilon}} \sqrt{2\pi m_\rho \frac{\rho\rho'}{\varepsilon}} e^{-m_\rho\rho\rho'/\varepsilon} I_m\left(m_\rho \frac{\rho\rho'}{\varepsilon}\right) \times e^{-m_\rho(\rho-\rho')^2/2\varepsilon}, \tag{11}$$

$$k^z(z,z';\varepsilon) = \sqrt{\frac{m_z}{2\pi\varepsilon}} e^{-m_z(z-z')^2/2\varepsilon}, \tag{12}$$

m_z and m_ρ are the effective masses for the motion along z and in the layer planes, respectively, $I_m(x)$ are the modified Bessel functions, and $V(\rho,z)$ is the potential. Therefore the eigenvalue equation (8) can be written as a tensorial product of one-dimensional matrices multiplied by a diagonal tensor. Finally, Eq. (8) is solved by a Lanczos-Arnoldi method.[23]

C. Coulomb corrections

If we neglect exciton-exciton interaction and use standard perturbation theory, we can estimate the Coulomb correction to the transition energy. In fact, the exciton binding energy E_C can be written

$$E_C = -\int d\mathbf{r}_e d\mathbf{r}_h \psi^{e*}_{(\alpha m)}(\mathbf{r}_e)\psi^{h*}_{(\alpha' m')}(\mathbf{r}_h)\frac{e^2}{4\pi\epsilon_0\epsilon_r}\frac{1}{|\mathbf{r}_e-\mathbf{r}_h|} \times \psi^{e}_{(\alpha m)}(\mathbf{r}_e)\psi^{h}_{(\alpha' m')}(\mathbf{r}_h), \tag{13}$$

where $\psi^e_{(\alpha m)}$ and $\psi^h_{(\alpha' m')}$ are the single-particle wave functions in the envelope function approximation. If we employ the Green function expansion formula and cylindrical coordinates, Eq. (13) becomes

$$E_C = -\frac{e^2}{4\pi\epsilon_0\epsilon_r}\sum_{l=0}^{+\infty} C^l, \tag{14}$$

where

$$C^l = \int d\rho_e d\rho_h dz_e dz_h \frac{(\rho^2+z^2)^{l/2}_<}{(\rho^2+z^2)^{(l+1)/2}_>} J^l_e(\rho_e,z_e)J^l_h(\rho_h,z_h) \tag{15}$$

and

$$J^l(\rho,z) = |\phi_{(\alpha m)}(\rho,z)|^2 P_l(z/\sqrt{\rho^2+z^2}). \tag{16}$$

Moreover, by using the expansion

$$\frac{r^l_<}{r^{l+1}_>} = \frac{r^l_e}{r^{l+1}_h}\theta(r_h-r_e) + \frac{r^l_h}{r^{l+1}_e}\theta(r_e-r_h), \tag{17}$$

we obtain

$$C^l = \int d\rho_e dz_e \{J^l_e(\rho_e,z_e)[(\rho_e^2+z_e^2)^{l/2}I^l_1(\rho_e,z_e) + (\rho_e^2+z_e^2)^{-(l+1)/2}I^l_2(\rho_e,z_e)]\}, \tag{18}$$

where

$$I^l_1(\rho_e,z_e) = \int d\rho_h dz_h (\rho_h^2+z_h^2)^{-(l+1)/2}J^l_h(\rho_h,z_h) \times \theta(\rho_h^2+z_h^2-\rho_e^2-z_e^2), \tag{19}$$

$$I^l_2(\rho_e,z_e) = \int d\rho_h dz_h (\rho_h^2+z_h^2)^{l/2}J^l_h(\rho_h,z_h) \times \theta(\rho_e^2+z_e^2-\rho_h^2-z_h^2). \tag{20}$$

These expressions can be computed numerically once the cylindrical wave functions, $\phi_{(\alpha m)}(\rho,z)$, are given. Then we can calculate the sum (14), which is rapidly converging.

III. NUMERICAL RESULTS AND DISCUSSION

In Fig. 4, we show the calculated electron and heavy-hole wave function projections along the z axis, for different layer separations. This figure clearly shows different localization properties of the electron and the heavy-hole wave functions. We see that the electrons are affected by the coupling between the stacked QD's already for layer separations of the order of 10 nm, while the heavy holes are affected by the coupling only for smaller GaAs spacer thicknesses. The implications of such a behavior of the carrier wave functions on the PL lifetimes in these structures have been already discussed in Ref. 5, and found to be in good agreement with the experimental data. In Ref. 5, however, the photoluminescence spectra were not fitted, since only the qualitative character, i.e., the relative localization properties of the electrons and the heavy holes, was important. Here we made a more accurate fitting with a more precise choice of the effective masses and the band offset in the potential model (see Ref. 15); as a result, the localization properties of the carrier wave functions turn out to be interchanged with respect to Ref. 5, but this fact does not affect the conclusions obtained there.

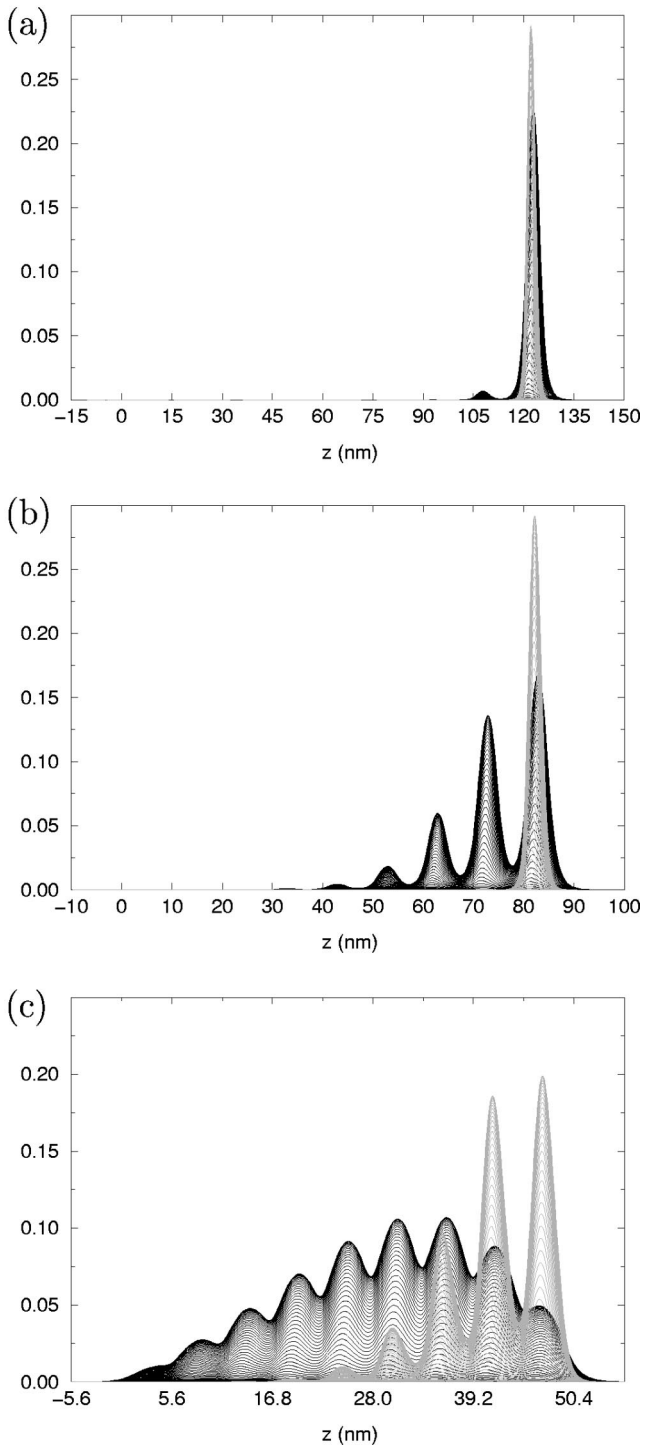

FIG. 4. Electron (black) and heavy-hole (gray) wave function projections along the z axis for an array of 9 staked QD's: (a) $D=15$ nm; (b) $D=10$ nm; (c) $D=5.6$ nm.

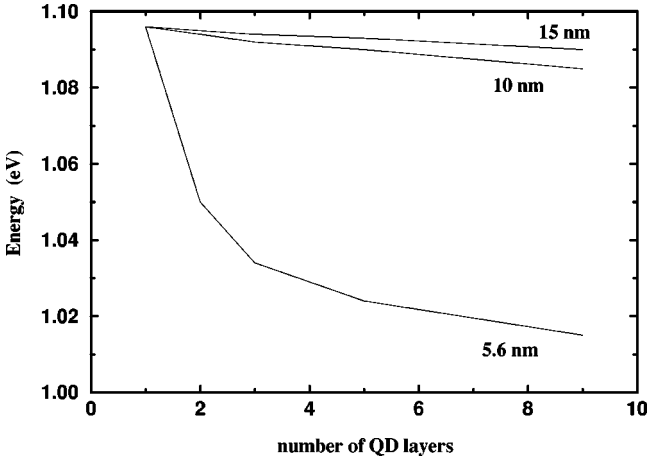

FIG. 5. Calculated fundamental transition energies without Coulomb corrections versus the number of QD layers for different layer separations.

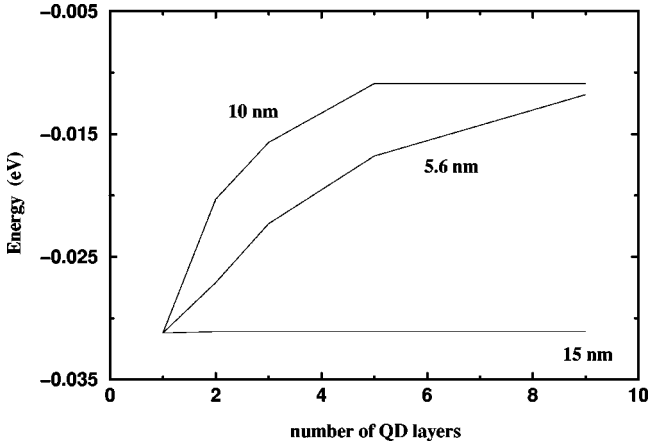

FIG. 6. Calculated Coulomb corrections versus the number of QD layers for different layer separations.

In Fig. 5, we show the calculated fundamental transition energies without Coulomb corrections versus the number of QD layers for different layer separations. This graph does not explain the blueshift and redshift of the photoluminescence spectra reported in Fig. 2. In fact, the different behavior of the fundamental transition energies with respect to different spacer thicknesses can be explained only by adding the electron-hole Coulomb interaction. This interaction decreases when the number of layers increases, due to the delocalization of the wave functions either of the electron alone or of the electron and the heavy hole together, in the intermediate [10 nm, Fig. 4(b)] or strong [5.6 nm, Fig. 4(c)] coupling regime, respectively. In Fig. 6, we plot an estimate of the Coulomb corrections versus the number of QD layers, for different layer separations. In the intermediate coupling regime, the plotted values are the averages of the corrections obtained for the different degenerate heavy-hole ground states.

The calculated fundamental transition energies with Coulomb corrections versus the number of QD layers for the layer separations of the actual samples are plotted in Fig. 2. The theoretical curves fit the experimental results quite well, at least for layer separations that are not too small. In the strong coupling regime, we do not have a good fit of the experimental data, as expected, but we still have a reasonable agreement.

We would like to note that, since the indium distribution in the QD is not uniform and the carrier wave functions are partially extended outside the QD island, the dielectric constant ϵ_r is a function of the position. In order to get a reasonable approximation, we used a value ($\epsilon_r \simeq 14$) between those of bulk InAs ($\epsilon_r = 15.2$) and bulk GaAs ($\epsilon_r = 12.5$). Finally, we observe that recent pseudopotential calculations have shown that the envelope function approximation overestimates the electron-hole Coulomb energy.[24] However, in QD's of this dimension these corrections do not change significantly the main features of our results.

CONCLUSIONS

We have investigated the effect of vertical coupling on the electronic levels and transition energies in multilayer InAs/GaAs quantum-dot structures, grown by ALMBE, as a function of the GaAs interlayer spacer thickness. Good agreement between the transition energies measured from the photoluminescence spectra and the calculations has been found, and the importance of taking into account the variation of the electron-hole Coulomb interaction as a function of the strength of the vertical coupling has been clearly shown.

ACKNOWLEDGMENTS

Work at LENS was supported by the European Community under the TMR Programme, Contract No. ERBFMGECT950017. This work was also supported by CNR-Progetto Finalizzato MADESS II.

[1] P. Frigeri, A. Bosacchi, S. Franchi, P. Allegri, and V. Avanzini, J. Cryst. Growth **201-202**, 1136 (1999).
[2] R. Heitz, M. Veit, N.N. Ledentsov, A. Hoffmann, D. Bimberg, V.M. Ustinov, P.S. Kop'ev, and Zh.I. Alferov, Phys. Rev. B **56**, 10 435 (1997).
[3] G.S. Solomon, J.P. Trezza, A.F. Marshall, and J.S. Harris, Jr., Phys. Rev. Lett. **76**, 952 (1996).
[4] K. Muraki, S. Fukatsu, Y. Shiraki, and R. Ito, Appl. Phys. Lett. **61**, 557 (1992).
[5] M. Colocci, A. Vinattieri, L. Lippi, F. Bogani, M. Rosa-Clot, S. Taddei, A. Bosacchi, S. Franchi, and P. Frigeri, Appl. Phys. Lett. **74**, 564 (1999).
[6] J.Y. Marzin and G. Bastard, Solid State Commun. **92**, 437 (1994).
[7] M. Grundmann, O. Stier, and D. Bimberg, Phys. Rev. B **52**, 11 969 (1995).
[8] H. Jiang and J. Singh, Phys. Rev. B **56**, 4696 (1997).
[9] C. Pryor, Phys. Rev. B **57**, 7190 (1998).
[10] M.A. Cusack, P.R. Briddon, and M. Jaros, Phys. Rev. B **54**, R2300 (1996).
[11] M.A. Cusack, P.R. Briddon, and M. Jaros, Phys. Rev. B **56**, 4047 (1997).
[12] D.M. Wood and A. Zunger, Phys. Rev. B **53**, 7949 (1996).

[13] A. Zunger, MRS Bull. **23** (2), 35 (1998).
[14] A.J. Williamson and A. Zunger, Phys. Rev. B **59**, 15 819 (1999).
[15] G. Cipriani, M. Rosa-Clot, and S. Taddei, Phys. Rev. B **61**, 7536 (2000).
[16] J.Y. Marzin, J.M. Gérard, A. Izraël, D. Barrier, and G. Bastard, Phys. Rev. Lett. **73**, 716 (1994).
[17] M. Berti, A.V. Drigo, A. Giuliani, M. Mazzer, A. Camporese, G. Rossetto, and G. Torzo, J. Appl. Phys. **80**, 1931 (1996).
[18] M. Colocci, F. Bogani, L. Carraresi, R. Mattolini, A. Bosacchi, S. Franchi, P. Frigeri, S. Taddei, and M. Rosa-Clot, Superlattices Microstruct. **22**, 81 (1997).
[19] M. Colocci, F. Bogani, L. Carraresi, R. Mattolini, A. Bosacchi, S. Franchi, P. Frigeri, M. Rosa-Clot, and S. Taddei, Appl. Phys. Lett. **70**, 3140 (1997).
[20] L.R.C. Fonseca, J.L. Jimenez, and J.P. Leburton, Phys. Rev. B **58**, 9955 (1998).
[21] M. Rosa-Clot and S. Taddei, Phys. Lett. A **197**, 1 (1995).
[22] S. Taddei, J. Comput. Phys. **134**, 62 (1997).
[23] R. B. Lehoucq, Argonne National Laboratory Report No. MCS-P591-0496 (1996) (unpublished).
[24] A. Franceschetti and A. Zunger, Phys. Rev. Lett. **78**, 915 (1997).